Combined Path Following and Vehicle Stability Control using Model Predictive Control

Lenssen, Daan; Bertipaglia, Alberto; Santafe, Felipe; Shyrokau, Barys

DOI
10.4271/2023-01-0645

Publication date
2023

Document Version
Final published version

Published in
SAE Technical Papers

2023-01-0645 Published 11 Apr 2023

Combined Path Following and Vehicle Stability Control using Model Predictive Control

Daan Lenssen and Alberto Bertipaglia Delft University of Technology

Felipe Santafe Toyota Motor Europe

Barys Shyrokau Delft University of Technology

Citation: Lenssen, D., Bertipaglia, A., Santafe, F., and Shyrokau, B., "Combined Path Following and Vehicle Stability Control using Model Predictive Control," SAE Technical Paper 2023-01-0645, 2023, doi:10.4271/2023-01-0645.

Received: 25 Oct 2022 Revised: 09 Jan 2023 Accepted: 09 Jan 2023

Abstract

This paper presents an innovative combined control using Model Predictive Control (MPC) to enhance the stability of automated vehicles. It integrates path tracking and vehicle stability control into a single controller to satisfy both objectives. The stability enhancement is achieved by computing two expected yaw rates based on the steering wheel angle and on lateral acceleration into the MPC model. The vehicle's stability is determined by comparing the two reference yaw rates to the actual one. Thus, the MPC controller prioritises path tracking or vehicle stability by actively varying the cost function weights depending on the vehicle states. Using two industrial standard manoeuvres, i.e. moose test and double lane change, we demonstrate a significant improvement in path tracking and vehicle stability of the proposed MPC over eight benchmark controllers in the high-fidelity simulation environment. The numerous benchmark controllers use different path tracking and stability control methods to assess each performance benefit. They are split into two groups: the first one uses differential braking in the control output, while the second group can only provide an equal brake torque for the wheels in the same axle. Furthermore, the controller's robustness is evaluated by changing various parameters, e.g. initial vehicle speed, mass and road friction coefficient. The proposed controller keeps the vehicle stable at higher speeds even with varying conditions.

Introduction

Following a target path and keeping the vehicle stable is a crucial property for active vehicle safety systems in automated driving. Vehicle stability control has reduced fatal single-vehicle accidents by about 30-50% for passenger cars and up to 50-70% for sport utility vehicles [1]. Despite this, the considerable uncertainty in the road friction coefficient and the potential conflicts between path tracking and stability performances make this problem particularly challenging [2]. If separate controllers perform each task, potential conflict between tracking and stability can happen. Thus, we focus on the combined control to mediate possible conflicting objectives with the primary of enhancing vehicle safety. Model Predictive Control (MPC) allows the simultaneous optimisation of the steering angle and the braking signal to perform evasive manoeuvres, and it improves the general performance of the controller [3]. For this reason, a vehicle driven at 14 m/s during an evasive manoeuvre can be stabilised by developing a nonlinear Model Predictive Control based on a 10 Degrees of Freedom (DoF) planar vehicle model [4]. However, its high complexity does not allow a real-time application because 12 s manoeuvres require a 15 min long simulation [4]. The complex 10 DoFs planar vehicle is substituted by an extended bicycle model, which has a better trade-off between simplicity and accuracy. It allows the computation of the yaw moment generated by the different tyre longitudinal forces in the same axle. Thus, it admits the application of differential braking as further control input together with the steering angle. The controller stabilises the vehicle in every situation, but its robustness to different vehicle masses and parameters is not assessed. Recently, a controller based on an integrated NMPC allowed direct computation of the control actions for each of the four wheels, assuring vehicle stability through constraints [2]. The controller robustness performance is extensively assessed by applying various disturbances, e.g. lateral wind, and varying the road friction coefficient. However, the stability and tracking objectives can clash during manoeuvres at the limit of the handling. In such a situation, assuring stability through constraints does not allow prioritising stability over tracking or vice versa. Therefore, in this paper, a combined approach covering path tracking and stability control into a single controller, using

the steering wheel, throttle and brakes as actuation, is proposed. The controller evaluates the vehicle's stability when deciding on the control inputs to follow the path. This leads to increased path tracking and stability compared to a control structure where separate controllers achieve these tasks. The combination is feasible thanks to the computation of two extra desired yaw rates on the steering wheel angle and on lateral acceleration. The actual yaw rate is compared with the two references, and the MPC controller prioritises path tracking or vehicle stability, varying the cost function weights. These parameters in the cost function differ depending on the vehicle state. A moose test and a double lane change in high-fidelity simulation environment are used to evaluate the performance of the proposed controller. Furthermore, its robustness is tested by varying the vehicle speed, the vehicle mass and the road friction coefficient.

The main contribution of this paper is twofold. The first is the combined path tracking and vehicle stability controller, which improves the tracking performance by 8% and enhances the vehicle stability by 11% compared with the baseline controllers. The second contribution is the improved robustness of the vehicle stability to the variation of vehicle speed, mass and road friction coefficient.

Proposed Controller

The following section explains the development of the proposed combined controller. It describes the nominal vehicle model, the reference generation, the stability assessment and the cost function weights tuning.

Vehicle Model

The vehicle motion is described by a planar vehicle model, see Figure 1. The model states are the longitudinal v_x and the lateral velocity v_y in the vehicle's body frame, the yaw rate $\dot{\psi}$, the longitudinal position X_p, the lateral position Y_p and the heading angle ψ in the global reference frame, the steering angle δ, the throttle position T_{hr} and the brake torque T_b. The model's inputs are the steering angle rate $\dot{\delta}$, the throttle rate $\dot{T}_{hr}$ and the brake torque rate $\dot{T}_b$. The dynamic equations of the vehicle model are represented as follows:

FIGURE 1 Planar vehicle model.

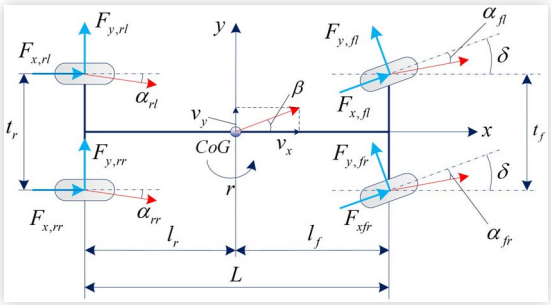

$$
\begin{aligned}
\dot{v}_x &= \frac{\left(F_{x,fl}+F_{x,fr}\right)\cos\left(\delta\right)-F_{drag}-\left(F_{y,fl}+F_{y,fr}\right)\sin\left(\delta\right)}{m}+\\
&+\frac{\left(F_{x,rl}+F_{x,rr}\right)}{m}+v_y\dot{\psi}\\
\dot{v}_y &= \frac{\left(F_{x,fl}+F_{x,fr}\right)\sin\left(\delta\right)+\left(F_{y,fl}+F_{y,fr}\right)\cos\left(\delta\right)}{m}+\\
&+\frac{\left(F_{y,rl}+F_{y,rr}\right)}{m}-v_x\dot{\psi}\\
\ddot{\psi} &= \frac{\left(F_{x,fl}+F_{x,fr}\right)\sin\left(\delta\right)l_f+\left(F_{y,fl}+F_{y,fr}\right)\cos\left(\delta\right)l_f+\left(F_{y,rl}+F_{y,rr}\right)l_r}{I_{zz}}+\\
&+\frac{0.5t_f\left(F_{x,fl}-F_{x,fr}\right)\cos\left(\delta\right)+0.5t_f\left(F_{y,fl}-F_{y,fr}\right)\sin\left(\delta\right)+0.5t_r\left(F_{x,rl}-F_{x,rr}\right)}{I_{zz}}\\
\dot{X}_p &= v_x\sin\left(\psi\right)+v_y\cos\left(\psi\right)\\
\dot{Y}_p &= v_x\sin\left(\psi\right)-v_y\sin\left(\psi\right)\\
&\dot{\psi}\\
&\dot{\delta}\\
&\dot{T}_{hr}\\
&\dot{T}_b
\end{aligned}
\tag{1}
$$

where $F_{x,ij}$ are the longitudinal tyre forces, i stands for front (f) or rear (r), while j stands for left (l) or right (r). $F_{y,\,ij}$ are the lateral tyre forces and F_{drag} is the aerodynamic drag force, which has quadratic relationship with the vehicle speed. The other parameters are reported in Table 1.

The longitudinal tyre forces are computed according to the following equations:

$$
F_{x,f}=\frac{G_R\left(\left(T_{rq,full}-T_{rq,\min}\right)T_{hr}+T_{rq,\min}\right)-\left(T_{b,fl}+T_{b,fr}\right)}{\mathrm{R}_{eff,f}} \tag{2}
$$

$$
F_{x,r}=-\frac{T_{b,rl}+T_{b,rr}}{\mathrm{R}_{eff,r}} \tag{3}
$$

where G_R is the total gear ratio between the engine and the wheels, $T_{rq,full}$ and $T_{rq,min}$ the maximum and minimum engine torque at the corresponding engine speed, $T_{b,ij}$ the

TABLE 1 Vehicle parameters used in the nominal model.

Symbol	Explanation	Value [Unit of measure]
l_f	Distance between the centre of gravity and the front axle	1.093 [m]
l_r	Distance between the centre of gravity and the rear axle	1.570 [m]
t_f	Front track width	1.628 [m]
t_r	Rear track width	1.635 [m]
m	Vehicle mass	1712 [kg]
I_{zz}	Vehicle inertia moment around the vertical axes	3386 [kg m^2]
$C_{l,fj}$	Cornering stiffness of front tyre	93468 [N rad]
$C_{l,rj}$	Cornering stiffness of rear tyre	76084 [N rad]
$C_{x,fj}$	Longitudinal stiffness of front tyre	211156 [N]
$C_{x,rj}$	Longitudinal stiffness of rear tyre	137764 [N]

braking torque on each wheel and $R_{eff,i}$ the effective tire radius at the front and rear axle of the vehicle. The engine torque map is defined as a look-up table.

The lateral tyre forces are computed as follow:

$$F_{y,fl} = C_{y,fl}\left(\delta - \frac{v_{y,fl}}{v_{x,fl}}\right) = C_{y,fl}\left(\delta - \frac{v_y + l_f\dot{\psi}}{v_x - 0.5t_f\dot{\psi}}\right) \tag{4}$$

$$F_{y,fr} = C_{y,fr}\left(\delta - \frac{v_{y,fr}}{v_{x,fr}}\right) = C_{y,fr}\left(\delta - \frac{v_y + l_f\dot{\psi}}{v_x + 0.5t_f\dot{\psi}}\right) \tag{5}$$

$$F_{y,rl} = C_{y,rl}\left(\delta - \frac{v_{y,rl}}{v_{x,rl}}\right) = C_{y,rl}\left(-\frac{v_y - l_r\dot{\psi}}{v_x - 0.5t_r\dot{\psi}}\right) \tag{6}$$

$$F_{y,rr} = C_{y,rr}\left(\delta - \frac{v_{y,rr}}{v_{x,rr}}\right) = C_{y,rr}\left(-\frac{v_y - l_r\dot{\psi}}{v_x + 0.5t_r\dot{\psi}}\right) \tag{7}$$

where $C_{y,ij}$ are the adaptive tyres cornering stiffness's computed at every time step according to the Dugoff tyre model, see Eq. 8. The Dugoff model is not differentiable, so it cannot be used during the MPC optimisation. Thus, the adaptive cornering stiffness is assumed to be constant over the prediction horizon in the MPC inner model [5]. The adaptive cornering stiffness allows to capture the non-linearities of the tire behaviour, so it increases the accuracy of the prediction, but it behaves such as linear tire model in the MPC inner model. The added complexity of a non-linear tyre model does not affect the optimisation time.

$$C_{y,ij} = C_{l,ij} f(\lambda_{ij}) \tag{8}$$

$C_{l,ij}$ are the tyre constant tyre cornering stiffness that are adapted at every time step by $f(\lambda)$, the weighting function of the Dugoff tyre model, see Eq. 9, which depends on the vehicle speed, road friction coefficient μ and the vertical force applied to the tyre $F_{z,ij}$ according to Eq. 10 and Eq. 11.

$$f(\lambda) = \begin{cases} \lambda(2-\lambda), & \lambda \le 1 \\ 1, & \lambda > 1 \end{cases} \tag{9}$$

$$\lambda = \frac{\mu F_{z,ij}(1-\kappa_{ij})}{2\sqrt{(C_{x,ij}\kappa_{ij})^2 + (C_{y,ij}\tan(\alpha_{ij}))^2}} \tag{10}$$

$$\mu = \mu_0\left(1 - e_r v_{x,ij}\sqrt{\kappa^2{}_{ij} + \tan^2(\alpha_{ij})}\right) \tag{11}$$

where κ_{ij} is the longitudinal slip of the front/rear left/right wheel, $C_{x,ij}$ is the longitudinal tyre stiffness, μ_0 is the peak friction coefficient and e_r is the friction reduction coefficient according to wheel longitudinal velocity.

Cost Function

The controller's objective is to follow a reference trajectory, keeping the desired speed and maintaining the vehicle inside the stability region. The proposed cost function is represented in Eq. 12. The number of equally spaced optimisation steps in the prediction horizon N is 30. All the symbols with foot N are related to the terminal stage of the MPC optimisation. R and R_r are the quadratic weights on the input and the input rate to reduce actuator's usage. Q_{V_X}, $Q_{\dot{\psi}}$, Q_y and Q_{ψ} are the quadratic weights for, respectively, longitudinal speed, yaw rate, lateral position and heading angle error. Their values ensure accurate path tracking to the controller but do not consider vehicle stability.

$$\begin{aligned} J = &\sum_{k=1}^{N-1}\begin{pmatrix} (V_{xi} - V_{xi,des})^2 Q_{V_x} + (\dot{\psi}_i - \dot{\psi}_{i,des})^2 Q_{\dot{\psi}} \\ +(y_i - y_{i,des})^2 Q_y + (\psi_i - \psi_{i,des})^2 Q_{\psi} \\ +(GY_{err,i})^2 Q_{GY_{err}} + (Ack_{err,i})^2 Q_{Ack_{err}} \\ +u_i{}^2 R + \dot{u}_i{}^2 R_r \end{pmatrix} + \\ &+\begin{pmatrix} (V_{xN} - V_{xN,des})^2 Q_{N,V_x} + (\dot{\psi}_N - \dot{\psi}_{N,des})^2 Q_{N,\dot{\psi}} \\ +(y_N - y_{N,des})^2 Q_{N,y} + (\psi_N - \psi_{N,des})^2 Q_{N,\psi} \\ +(GY_{err,N})^2 Q_{N,GY_{err}} + (Ack_{err,N})^2 Q_{N,Ack_{err}} \\ +u_N{}^2 R_N \end{pmatrix} \end{aligned} \tag{12}$$

$Q_{GY_{err}}$ and $Q_{Ack_{err}}$ are, respectively, the quadratic weights on the error between the actual yaw rate and two expected steady state yaw rates, one based on the vehicle lateral acceleration GY_{err} and the other one based on steering wheel angle Ack_{err}. The first error is computed according to the following equation:

$$GY_{err} = \frac{a_y}{v_x} - \dot{\psi} \tag{13}$$

The second one is computed according to the following:

$$Ack_{err} = \frac{\delta v_x}{L(1 + k_h v_x{}^2)} - \dot{\psi} \tag{14}$$

where k_h is the stability factor [6], computed according to:

$$k_h = \frac{m}{L}\left(\frac{\frac{l_f C_{y,f} - l_r C_{y,r}}{-C_{y,f} - C_{y,r}}}{-l_f C_{y,f} - \frac{l_f C_{y,f} - l_r C_{y,r}}{C_{y,f} + C_{y,r}} C_{y,f}}\right) \tag{15}$$

FIGURE 2 $Q_{GY_{err}}$ and $Q_{Ack_{err}}$ multiplication factor based on the vehicle state β- $\dot{\beta}$ phase plot.

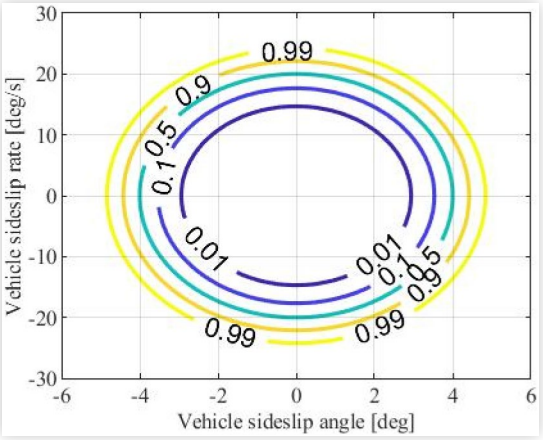

The value of the front and rear cornering stiffness ($C_{y,f}$ $C_{y,r}$) are adapted at every time step as described in Eq. 9, Eq. 10 and Eq. 11 of section "Vehicle Model".

GY_{err} and Ack_{err} aim to keep the vehicle in a steady state condition, enhancing its stability. Thus, there are three yaw rates that the MPC will optimise for: i) yaw rate related to path curvature, ii) yaw rate related to the steering input and iii) yaw rate related to the lateral acceleration. The first one, associated tuning weight $Q_{\dot{\psi}}$, is related to path tracking, and its mathematical definition is provided in Eq. 19, while the other two are related to vehicle stability. However, clashes between tracking and stability occur during manoeuvres at the limit of handling. Thus, $Q_{GY_{err}}$, $Q_{Ack_{err}}$ and $Q_{\dot{\psi}}$ are varied along the vehicle manoeuvre to prioritise tracking or stability. The weights associated with GY_{err} and Ack_{err} change depending on the vehicle's sideslip angle β and sideslip angle rate $\dot{\beta}$. The vehicle sideslip angle cannot be measured through the sensors currently installed in the commercial vehicle, so it is estimated [7, 8]. $Q_{GY_{err}}$, $Q_{Ack_{err}}$ are multiplied by the same factor between 0 and 1, computed according to Figure 2. When the vehicle has low β and $\dot{\beta}$ values, the multiplication factor is close to 0 because the vehicle is already stable, hence, $Q_{GY_{err}}$, $Q_{Ack_{err}}$ are much lower than $Q_{\dot{\psi}}$. Thus, the MPC controller prioritises path tracking over vehicle stability. Vice versa, when the vehicle has a high β and $\dot{\beta}$ values, the multiplication factor is close to 1 because the vehicle is close to the unstable region. Thus, the MPC controller prioritises vehicle stability over path tracking. This cost function adaptivity differentiate the proposed approach from the available literature. The circular shape of the multiplication factor correspond to the circle circumscribed in the stability trapezoid, usually associated with the phase-plot analysis [9, 10]. This assumption is conservative, but it further prioritises stability over path tracking, reducing the chances that the controller brings the vehicle into an unstable region. All the tuned weight coefficient are reported in the Appendix.

Constraints

The implemented constraints are:

$$
\begin{aligned}
0 \le v_x \le \frac{170}{3.6} \\
0 \le T_{hr} \le 1 \\
-1 \le \dot{T}_{hr} \le 1 \\
-2.76\frac{360\pi}{180 S_{rat}} \le \delta \le 2.76\frac{360\pi}{180 S_{rat}} \\
-\frac{800\pi}{180 S_{rat}} \le \dot{\delta} \le \frac{800\pi}{180 S_{rat}} \\
0 \le T_b \le 4886 \\
-7023 \le \dot{T}_b \le 7023
\end{aligned}
\tag{16}
$$

The equality constraint ensures that the optimisation follows the dynamics of the planar vehicle model. The goal of the inequality constraints is to limit the maximum values and the maximum rates of the control outputs. From top to bottom, the first constraint limits the velocity to the vehicle's top speed. The second and third constraints limit the throttle input and throttle rate, respectively. The throttle input is limited between 0 and 1, where 0 means the throttle is closed, while 1 corresponds to a fully open throttle. The throttle rate is limited to ensure smooth driving. Furthermore, the steering wheel angle and steering wheel angle rate are also constrained, and their values depend on the steering ratio S_{rat} (18.8). The final two constraints limit the brake torque and the brake torque rate.

Benchmark Controllers, KPIs and Manoeuvres

This section describes the baseline methods, selected KPIs and manoeuvres.

Benchmark

The proposed solution is compared with eight benchmark controllers, representing different baselines for path tracking, stability control and a cascade of the two. Furthermore, every baseline is designed with or without differential braking. They are mainly split into two sets. The first one, called Single Brake (SB), is a control architecture where the braking input is a single brake command to all wheels. The second set, called Differential Braking (DB), is formed by controllers that apply differential braking and thus independently send different brake pressure to each wheel. This makes the controller more complex but gives the ability to induce an extra yaw moment to the vehicle. Every control set is further split into four groups:

- Path Tracking (PT): it performs path tracking without considering vehicle stability. The controller uses the lateral position, the yaw angle and the vehicle speed as references.
- Path Tracking and Yaw Rate (PTY): it adds to the simple path tracking controller a reference yaw rate, based on

the path curvature and vehicle speed, in the cost function to develop the stability control capabilities.

- Path Tracking & Stability Constraints (PTC): it is a path tracking controller which adds two constraints to the MPC formulation to ensure vehicle stability. The combination of path tracking and stability constraints aims to develop a controller capable of correctly following a path, even in emergency manoeuvres, keeping the vehicle stable in every situation. The further constraint limits the error between the actual vehicle yaw rate and the expected yaw rate.
- Path Tracking & Stability Controller (PTS): a cascade controller in which the path tracking MPC, from the first configuration, is followed by a separate stability controller. The latter is a simplified version of industrial vehicle stability controller.

KPIs

The performance of every controller is assessed using five KPIs, commonly used for path tracking and vehicle stability controllers [4, 11, 12]. The proposed KPIs are:

- The Normalised Root Mean Square Error (NRMSE) of the lateral position $NRMSE_y$, heading angle $NRMSE_\psi$, and yaw rate $NRMSE_{\dot{\psi}}$ to evaluate the tracking performance.
- The Root Mean Square Error (RMSE) of the difference between the expected yaw rate, based on the steering angle $RMSE_{Ack}$, and the actual vehicle yaw rate to assess vehicle stability.
- The RMSE of the difference between the expected yaw rate, based on the lateral acceleration $RMSE_{GY}$, and the actual vehicle yaw rate to analyse vehicle stability.
- The average vehicle speed (Mean_Vx) during the manoeuvre to evaluate that tracking and stability performance differences between the controllers are due to the inherent properties of the applied methodologies and not a more invasive braking action.

The computation of all the KPIs starts as soon as the vehicle enters in track designed for the Double Lane Change or Moose manoeuvre.

Manoeuvres

Two manoeuvres used to evaluate the performance of the proposed controller: i) Double Lane Change, and ii) Moose test, designed following ISO 3888-1 and ISO 3888-2. Both represent evasive manoeuvres when the vehicle has to avoid an object crossing the vehicle's path [11, 13]. The main differences between the two tests are the road's length and the lanes' width. While the vehicle drives for 125 m to complete a double lane change, the length of a moose test is only 61 m. Thus, the track's width is slightly wider in a moose manoeuvre. Furthermore, the initial velocity in Double Lane Change test is 80 km/h, while it is 72 km/h in the Moose test. However, the Moose test is a more challenging manoeuvre [14]. The reference velocity is considered constant along all the trajectory. For both manoeuvres, the path is generated using two consecutive sigmoid curves that relate the longitudinal position to a lateral offset [15]. The following equation gives the desired lateral position:

$$y_{des}(x) = \frac{P_b}{1 + e^{-P_a(x - P_c)}} \tag{17}$$

where P_a, P_b and P_c are parameters used to define the curve. Two sigmoid curves in opposite directions generate the two sequential corners. The generated manoeuvres are used to compute the reference yaw angle ψ_{des}, see Eq. 17, and the reference yaw rate $\dot{\psi}_{des}$, see Eq.19.

$$\psi_{des} = \arctan\left(\frac{\partial y_{des}}{\partial x}\right) \tag{18}$$

Where $\frac{\partial y_{des}}{\partial x}$ is the derivative of the lateral reference position over the derivative of the longitudinal vehicle position, computed according to:

$$\frac{dy_{des}}{dx} = \frac{P_a P_b e^{-P_a(x - P_c)}}{\left(1 + e^{-P_a(x - P_c)}\right)^2} \tag{19}$$

$$\dot{\psi}_{des} = k v_x \tag{20}$$

Where k is the curvature of the road, which is computed according to the following equation:

$$k = \frac{\left(\frac{\partial^2 y_{ref}}{\partial x^2}\right)}{\left(1 + \left(\frac{\partial y_{ref}}{\partial x}\right)^2\right)^{\frac{3}{2}}} \tag{21}$$

Double Lane Change Variations

Several variations are applied to the Double Lane Change test, to evaluate the robustness of the controllers, such as road friction coefficient, initial vehicle speed, and vehicle weight variation. The summary of all the simulated conditions is summarized in Table 2.

Three different initial velocities are considered: 70 km/h, 80 km/h and the maximum speed for which the controller is capable of keeping the vehicle inside the road boundaries.

Two additional weights are added to the vehicle: 150 kg and 300 kg. In the case of 150 kg, the extra weight is equally split between the driver and passenger locations. While in the case of 300 kg, the weight is added also to the left- and right-rear passenger locations. These variations aim to analyse how additional passengers influence the controller's performance.

The road friction coefficient variations are considered for two different scenarios. In the first one, the μ level of the whole

TABLE 2 Summary of the different initial conditions for a double lance change manoeuvre.

Number of variations	Friction Coeff. [-]	Initial Vehicle Velocity [km/h]	Added Weight [kg]
1	0.9	70	0
2	0.9	80	0
3	0.9	Max	0
4	0.9	80	150
5	0.9	80	300
6	0.3	70	0
7	0.6	80	0
8	0.9 to 0.6	80	0
9	0.6 to 0.9	80	0
10	0.6 to 0.3	70	0
11	0.3 to 0.6	70	0

road changes. It emulates different road conditions such as ice or snow ($\mu = 0.3$), rain ($\mu = 0.6$) and dry ($\mu = 0.9$). The icy road's initial velocity is reduced to 70 km/h because none of the controllers complete the manoeuvre with a higher initial speed. The second scenario shows a difference in μ level between the two lanes. The initial velocity is set up to 70 km/h whenever the road has a friction coefficient of 0.3 because it represents the highest speed for which all controllers successfully pass the manoeuvre.

Simulation Results

Experiments are conducted with a passenger vehicle modelled in IPG/Carmaker using a high-fidelity Toyota vehicle model. The model has been parametrized based on mass-inertia parameters obtained from vehicle inertia measuring facility, suspension kinematics and compliance obtained by measurement on a Kinematics & Compliance test rig for wheel suspension characterization, and finally, validated by field tests on the proving ground. This section demonstrates the performance of the proposed controller concerning the benchmark methods. The analysis is performed by simulating the Moose test. Furthermore, it studies the robustness of the proposed controller using different vehicle and road conditions in the Double Lane Change test.

Moose Test

The vehicle's trajectory obtained by different controllers configuration in the Moose test is shown in Figure 3. All the controllers allow the vehicle to pass the test successfully but with different performance levels. Thus, a focus on the vehicle lateral tracking error is reported in Figure 4. It shows that the SB-PTC controller has the highest overshoot when moving to the offset lane, while the proposed controller has the lowest one. Interestingly, the DB-PTS controller shows the lowest overshoot when returning to the original lane. In general, Figure 3 and Figure 4 prove that controllers with differential braking have a lower overshoot and allow a tighter turn to the

FIGURE 3 Vehicle trajectory for the Moose test at 72 km/h.

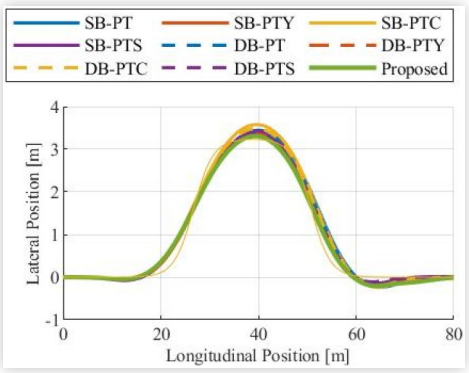

FIGURE 4 Lateral tracking error for the Moose test at 72 km/h.

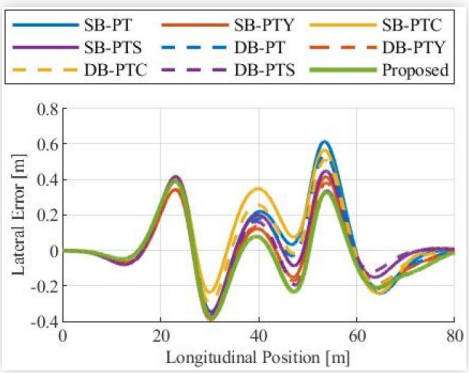

vehicle. This is due to the extra yaw moment generated by the different braking torque of the left and right tyres. Despite the different braking actions of every controller, the different Mean_Vx of each controller is in a range lower than 1 km/h. Thus, the different tracking and stability performances between the controllers are due to their inner properties. Despite the similarity of Mean_Vx, it is important to highlight that the minimum average velocity along the moose test is always found for the cascaded controllers with and without differential braking.

A further analysis of the path tracking capabilities is reported in Figure 5. It evaluates the controller performance by comparing the $NRMSE_y$ and $NRMSE_\psi$. Both values are better when they are minimised. It can be seen that the controllers with the best performance are the proposed controller and DB-PTY, closely followed by SB-PTY. It is necessary to investigate the vehicle's stability properties with tracking capabilities (see Figure 6). The cascaded controller configuration with and without differential braking achieves higher stability properties, closely followed by the SB-PTC controller. By analysing Figure 5 and Figure 6, differential braking helps the controller achieve higher tracking performance at the cost of stability.

However, the relative performance changes when performing the Moose test at the maximum speed for which each controller still completes the manoeuvre. Figure 7 and Figure 8 show, respectively, the controller path tracking and

FIGURE 5 Comparison of the controllers path tracking capabilities using $NRMSE_y$ and $NRMSE_\psi$ (Moose test, 72 km/h).

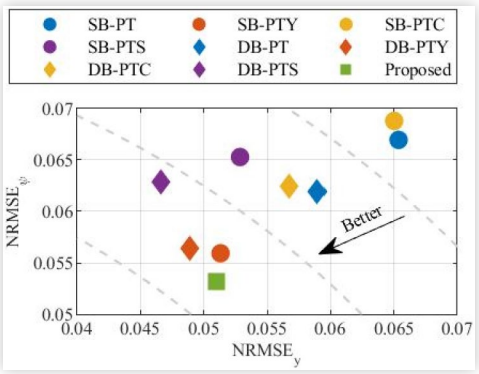

FIGURE 6 Comparison of the controllers stability capabilities using $RMSE_{Ack}$ and $RMSE_{GY}$ (Moose test, 72 km/h).

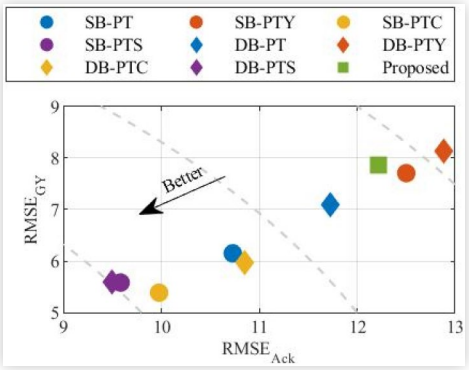

FIGURE 7 Comparison of the controllers path tracking capabilities using $NRMSE_y$ and $NRMSE_\psi$ (Moose test, maximum speed).

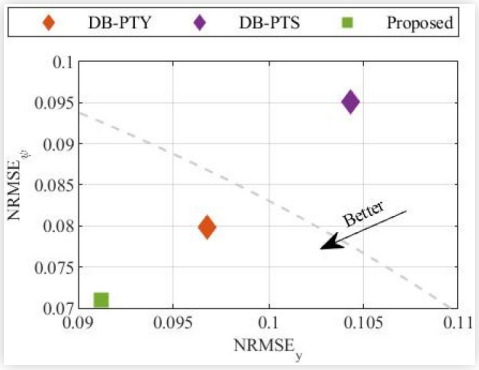

stability performance in the Moose test driven at the maximum velocity. In this scenario, it can be seen that the proposed controller achieves the best performance for both path tracking and stability compared with DB-PTY and DB-PTS. The performance improvement for the stability KPIs of the proposed controller is 11% over the DB-PTS. While the improvement for the tracking KPIs is 8% over the DB-PTY in the maximum speed scenario.

FIGURE 8 Comparison of the controllers stability capabilities using $RMSE_{Ack}$ and $RMSE_{GY}$ (Moose test, maximum speed).

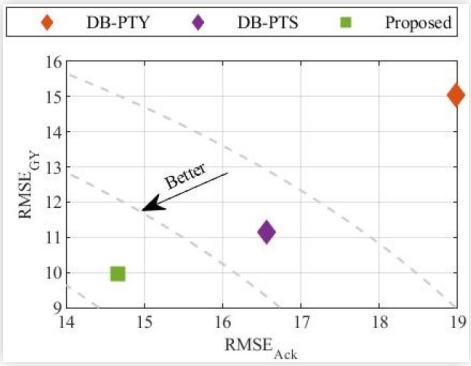

FIGURE 9 $\beta - \dot{\beta}$ phase portrait for the proposed controller, DB-PTC and DB-PTS (Moose test, maximum speed).

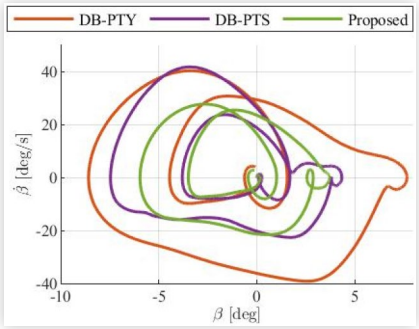

The stability properties can also be compared considering the sideslip angle and sideslip angle rate phase portrait, see Figure 9. The proposed controller has significantly lower β and $\dot{\beta}$ values, with a maximum β of 6 deg and a maximum $\dot{\beta}$ of 30 deg/s. These values coincide with the stability prioritisation in the proposed controller. It highlights the ability of the proposed controller to prioritise tracking or stability depending on the state of the vehicle.

Double Lange Change

This section focuses on the robustness of the proposed controller showing how the tracking and stability KPIs change at the variations of initial speed, mass and friction coefficient in the Double Lane Change manoeuvre.

Initial Velocity Variation Figure 10 shows the variation of the tracking KPIs in the Double Lane Change test with a different velocity. All the controllers have a linear increase in the KPIs when the velocity increases. SB-PTC and DB-PTC show the steepest KPIs increase, and they have the lowest maximum speed at which the vehicle successfully performs the manoeuvre. Furthermore, the controllers with differential braking improved tracking performance at the cost of stability, see Figure 11. At lower speeds, the lateral tracking performance of the proposed controller is slightly worse than the

FIGURE 10 Tracking KPIs variation according to initial velocity.

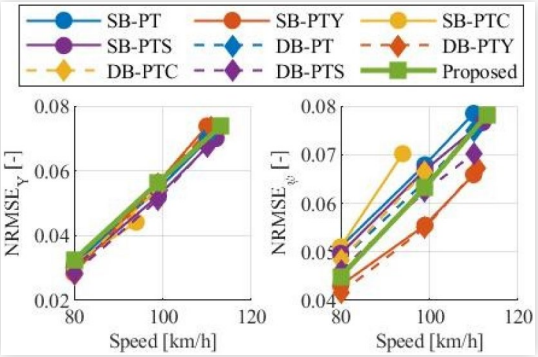

FIGURE 11 Stability KPIs variation according to initial velocity.

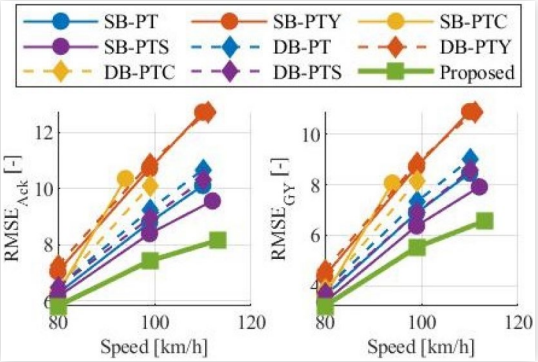

other controllers, but at higher speeds, it outperforms all the others. Furthermore, it allows the vehicle to be driven with the highest speed within the road bounds of the Double Lane Change manoeuvre. Figure 10b shows the tracking of the heading angle. The path-tracking performance of the proposed controller deteriorates more at higher speeds than the other controllers. This can be explained by looking at the two stability KPIs (Figure 11). The proposed controller has better stability performance at all speeds, with a lower performance deterioration at higher speeds as well. The reference yaw rate, based on the path curvature, is challenging to track at higher speeds without compromising stability. Therefore better stability KPIs will result in overall lower yaw tracking KPIs.

Vehicle Weight Variations The variation of the tracking and stability KPIs due to adding weight is shown in Figure 12 and Figure 13. The added weight causes worse performance for all controllers. However, the tracking performance of the controllers with differential braking is less affected than the ones without it. Considering vehicle stability, the opposite trend is noticeable. Nevertheless, there are some outliers. For instance, the DB-PTY controller has a better $RMSE_{ack}$ with further mass of 300 kg than 150 kg. Another example is the SB-PT controller, which has a better $RMSE_{Gy}$ at 150kg than with no extra weight. However, the overall performance of DB-PTY and SB-PT still deteriorates when looking at the combined $RMSE_{ack}$ and $RMSE_{Gy}$ performance. The most

FIGURE 12 Tracking KPIs variation due vehicle weight.

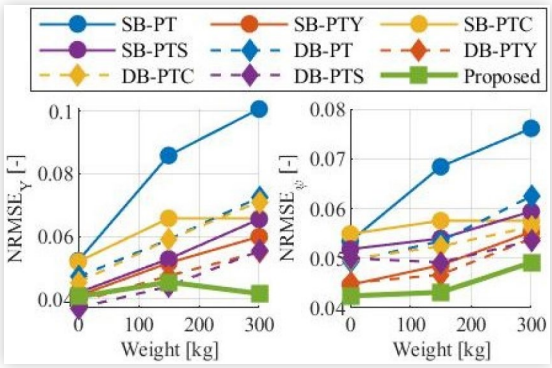

FIGURE 13 Stability KPIs variation due vehicle weight.

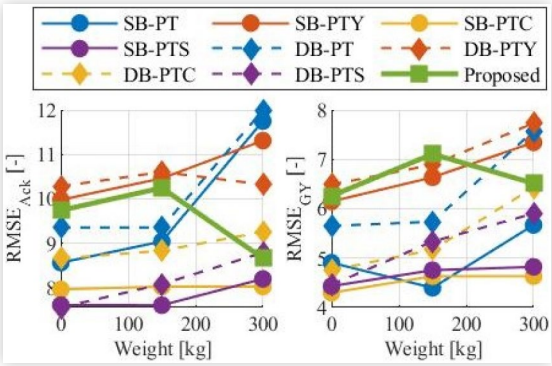

notable observation about the proposed controller is that almost all KPIs have a drop when going from 150 kg to 300 kg. This indicates a better performance when 300 kg is added instead of only 150 kg. All the other controllers show the opposite trend.

Friction Coefficient Figure 14 and Figure 15 show, respectively, the tracking and stability KPIs variation when the manoeuvre is simulated with various friction coefficient. When lowering μ, the controllers generally have worse tracking performance. Regarding stability, there is a clear performance gap between the controllers that can use

FIGURE 14 Tracking KPIs variation due to friction coefficient.

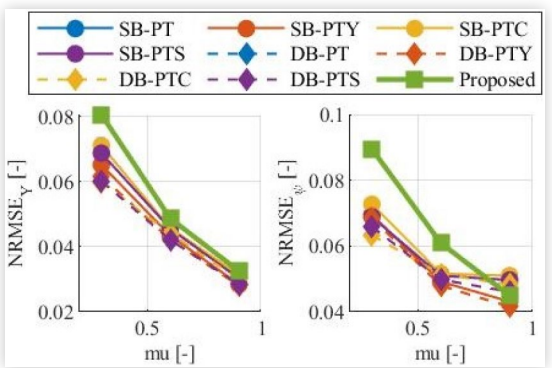

FIGURE 15 Stability KPIs variation due to friction coefficient.

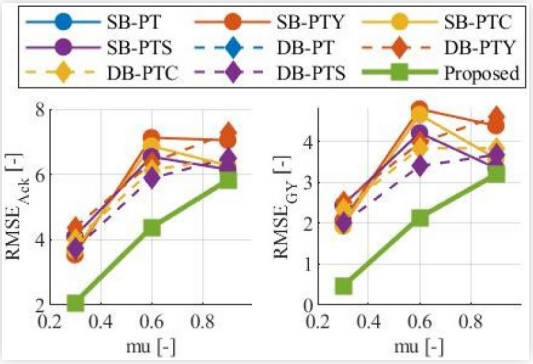

differential braking and those that cannot. The controllers with differential braking have better stability in the 0.6μ case compared to the 0.9μ case, while those without DB have worse stability in the 0.6μ case. However, when μ is equal to 0.3, the controllers without differential braking have slightly better stability performance than the others. It is essential to highlight that the worst stability KPIs in the 0.3μ case is partly due to the lower initial speed for this scenario, see Figure 15. Analysing the tracking KPIs, there is a difference between the controllers with and without differential braking. The controllers with DB have lower tracking performance deterioration in the lower μ conditions, see Figure 14. A possible explanation is that the front wheels quickly reach the saturation region at the low friction scenario. There is a more significant deterioration in tracking performance for the proposed controller than for the other controllers. However, the stability of the vehicle also increased the most. It is important to highlight that with a different controller tuning for low μ scenarios, the tracking could be improved at the cost of stability. For safety reasons, it is preferred to insure vehicle stability.

Split Friction Coefficient Figure 16 and Figure 17 show the results for the split friction coefficient scenario. The controllers with differential braking perform better than the controllers without it in all cases. A possible explanation is that DB controllers have an extra control input available to control the vehicle. Furthermore, the performance for all

FIGURE 16 Tracking KPIs variation when the road has a split friction coefficient.

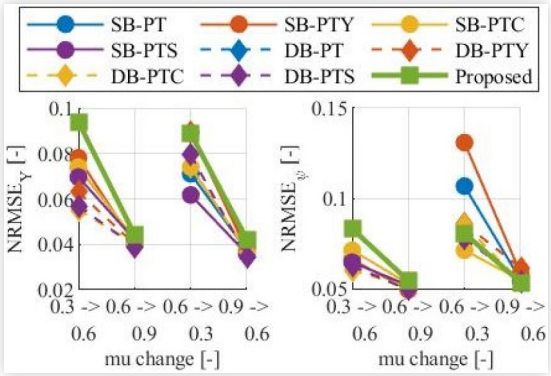

FIGURE 17 Stability KPIs variation when the road has a split friction coefficient.

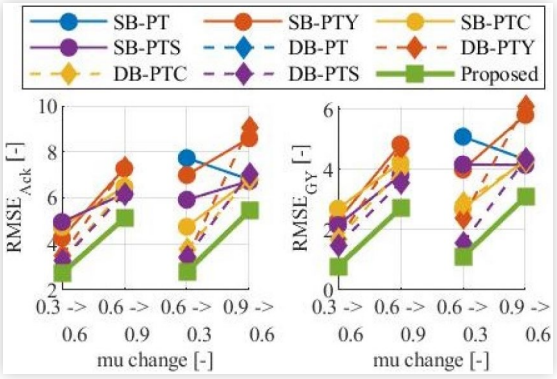

controllers is better in the scenario where the original lane has a lower μ than the second lane. A possible explanation is that the controller predicts a particular input expecting a low friction coefficient μ, but when the μ level suddenly increases, more grip is available, making the path easier to follow. In the opposite scenario, the reverse is true. When the μ level suddenly lowers, there is less grip available, which the controller could not previously predict. The vehicle is more difficult to control and reduces tracking and stability. For most KPIs, the relative performance between the controllers remains similar for the different scenarios. One exception happens in the tracking KPIs where the proposed controller has a much more significant decrease in performance in the 0.3 → 0.6μ scenario. In this situation, the proposed controller has better stability at the cost of worse tracking, as it happens when the entire road has a low friction coefficient.

Conclusions

This paper presents a novel MPC controller which combines path tracking and vehicle stability into a single controller. It includes two additional reference yaw rates to the cost function, indicating the vehicle's stability. The performance of the proposed control is compared with eight benchmarks designed to evaluate the benefits of different path tracking and stability controllers. Their performance is assessed through two industry-standard tests, i.e. Moose test and Double Lane Change. Furthermore, the controller's robustness is tested by changing various vehicle and road parameters in the Double Lane Change manoeuvre. Using the high-fidelity simulation environment, it is shown that adding differential braking increases the overall performance of the controllers. The path tracking performance is increased at the cost of a slight decrease in stability performance. Additionally, the controllers with differential braking are more robust in varying conditions. Primarily, we prove an 8% improvement in tracking capability and an 11% improvement in stability performance than a cascaded controller path tracking and vehicle stability with differential braking. Furthermore, it also has the best robustness to the considered variations. Future

works involve the implementation of the proposed controller in a vehicle demonstrator to verify its benefit in a real scenario.

References

1. Ferguson, S.A., "The Effectiveness of Electronic Stability Control in Reducing Real-World Crashes: A Literature Review," *Traffic injury prevention* 8, no. 4 (2007): 329-338.
2. Chowdhri, N., Ferranti, L., Iribarren, F.S., and Shyrokau, B., "Integrated Nonlinear Model Predictive Control for Automated Driving," *Control Engineering Practice* 106 (2021): 104654.
3. Falcone P., Borrelli F., Asgari J., Tseng E., and Hrovat D., "Predictive Active Steering Control for Autonomous Vehicle Systems," *Control Systems Technology, IEEE Transactions on*, 15, 566-580, 06/01 2007, 10.1109/TCST.2007.894653.
4. Falcone, P., Eric Tseng, H., Borrelli, F., Asgari, J. et al., "MPC-Based Yaw and Lateral Stabilisation Via Active Front Steering and Braking," *Vehicle System Dynamics* 46, no. S1 (2008): 611-628.
5. Bhoraskar A. and Sakthivel P., "A Review and a Comparison of Dugoff and Modified Dugoff Formula with Magic Formula," in *2017 International Conference on Nascent Technologies in Engineering (ICNTE)*, 27–28 Jan. 2017, 2017, 1-4, 10.1109/ICNTE.2017.7947898.
6. Milliken W., Milliken D., Kasprzak E., and Metz L., "Race Car Vehicle Dynamics: Problems, Answers and Experiments," *Dynamics*, 265, 5Control267, 1995.
7. Bertipaglia A., de Mol D., Alirezaei M., Happee R., and Shyrokau B., "Model-Based Vs Data-Driven Estimation of Vehicle Sideslip Angle and Benefits of Tyre Force Measurements," *arXiv preprint arXiv: 2206.15119*, 2022.
8. Bertipaglia A., Shyrokau B., Alirezaei M., and Happee R., "A Two-Stage Bayesian Optimisation for Automatic Tuning of an Unscented Kalman Filter for Vehicle Sideslip Angle Estimation," in *Proc. of 33rd IEEE Intelligent Vehicles Symposium*, Aachen, Germany, 2022.
9. Shyrokau B. and Wang D., "Control Allocation with Dynamic Weight Scheduling for Two-Task Integrated Vehicle Control,"in *Proc. 11th Int. Symp. Adv. Vehicle Control*, 2012, 1-6.
10. Shyrokau, B., Wang, D., Savitski, D., Hoepping, K. et al., "Vehicle Motion Control with Subsystem Prioritization," *Mechatronics* 30 (2015): 297-315.
11. Li, L., Lu, Y., Wang, R., and Chen, J., "A Three-Dimensional Dynamics Control Framework of Vehicle Lateral Stability and Rollover Prevention Via Active Braking with MPC," *IEEE Transactions on Industrial Electronics* 64, no. 4 (2016): 3389-3401.
12. Zhang, W., Wang, Z., Drugge, L., and Nybacka, M., "Evaluating Model Predictive Path Following and Yaw Stability Controllers for over-Actuated Autonomous Electric Vehicles," *IEEE Transactions on Vehicular Technology* 69, no. 11 (2020): 12807-12821.
13. Lu, H., Shi, Y., He, D., and Yu, F., "Model-Based Vehicle Stability Control with Tyre Force and Instantaneous Cornering Stiffness Estimation," *Proceedings of the Institution of Mechanical Engineers, Part D: Journal of Automobile Engineering* 230, no. 6 (2016): 754-770.
14. Guo R.Q., Yuan L., and Xie J.Z., "Implement of Handling and Stability Road Test of Passenger Vehicle for ISO Standards," *Applied Mechanics and Materials*, 2014, 568: Trans Tech Publ, 1869-1874.
15. Lu, B. et al., "Hybrid Path Planning Combining Potential Field with Sigmoid Curve for Autonomous Driving," *Sensors* 20, no. 24 (2020): 7197.

Contact Information

Alberto Bertipaglia is with the Department of Cognitive Robotics, Delft University of Technology, 2628 CD Delft, The Netherlands.
A.Bertipaglia@tudelft.nl

Acknowledgments

The Dutch Science Foundation NWO-TTW supports the research within the EVOLVE project (nr. 18484).

Abbreviation

MPC - Model Predictive Control
KPI - Key Performance Indicator
NRMSE - Normalised Root Mean Squared Error
RMSE - Root Mean Squared Error
DB - Differential Braking
SB - Single Braking
PT - Path Tracking
PTY - Path Tracking and Yaw Rate
PTC - Path Tracking & Stability Constraints
PTS - Path Tracking & Stability Controller
Mean_Vx - Mean longitudinal Velocity of the vehicle

Appendix

Tuning coefficient	Value	Tuning coefficient	Value
Q_V	$1e1/\mu^5$	$Q_{N,V}$	$1e2/\mu^6$
Q_y	$5e3/\mu$	$Q_{N,y}$	$5e4/\mu^2$
Q_ψ	$3e4/\mu$	$Q_{N,\psi}$	$5e5/\mu^4$
Q_r	$3e3/\mu$	$Q_{N,r}$	$1e3/\mu^2$
Q_{st}	$5e3/\mu^3$	$Q_{N,st}$	$5e3/\mu^6$
Q_{Br}	$1e-3/\mu^3$	$Q_{N,Br}$	$1e-2/\mu^3$
Q_{Thr}	$1e3/\mu^3$	$Q_{N,Thr}$	$1e4/\mu^3$
$R_{\Delta st}$	$5e3/\mu^6$	$R_{N,\Delta st}$	-
$R_{\Delta Br}$	$5e-5/\mu^5$	$R_{N,\Delta Br}$	-
$R_{\Delta Thr}$	$1e3/\mu^3$	$R_{N,\Delta Thr}$	-
$Q_{Ack,err}$	$AF * 1e4/\mu^{4.75}$	$Q_{N,Ack,err}$	$AF * 1e4/\mu^{4.75}$
$Q_{GY,err}$	$AF * 1e6/\mu^{2.5}$	$Q_{N,GY,err}$	$AF * 1e6/\mu^{2.5}$

ISSN 0148-7191